A TWO-PHASE HEAT SPREADER FOR COOLING HIGH HEAT FLUX SOURCES

Mitsuo Hashimoto, Hiroto Kasai, Yuichi Ishida, Hiroyuki Ryoson, [a]
Kazuaki Yazawa, [b]
Justin A. Weibel, Suresh V. Garimella [c]
[a] Sony Corporation, 6-7-35 Kitashinagawa Shinagawa-ku, Tokyo, 141-0001 Japan
(81) 3-5448-6572, Mitsuo.Hashimoto@jp.sony.com
[b] Electrical Engineering Dept., University of California Santa Cruz, 1156 High St, Santa Cruz, CA 95064 USA
[c] School of Mechanical Engineering, Purdue University, West Lafayette, IN 47907-2088 USA

ABSTRACT

A two-phase heat spreader has been developed for cooling high heat flux sources in high-power lasers, high-intensity light-emitting diodes (LEDs), and semiconductor power devices. The heat spreader uses a passive mechanism to cool heat sources with fluxes as high as 5 W/mm^2 without requiring any active power consumption for the thermal solution. The prototype is similar to a vapor chamber in which water is injected into an evacuated, air-tight shell. The shell consists of an evaporator plate, a condenser plate and an adiabatic section. The heat source is made from aluminum nitride, patterned with platinum. The heat source contains a temperature sensor and is soldered to a copper substrate that serves as the evaporator. Tests were performed with several different evaporator microstructures at different heat loads. A screen mesh was able to dissipate heat loads of 2 W/mm^2, but at unacceptably high evaporator temperatures. For sintered copper powder with a 50 μm particle diameter, a heat load of 8.5 W/mm^2 was supported, without the occurrence of dryout. A sintered copper powder surface coated with multi-walled carbon nanotubes (CNT) that were rendered hydrophilic showed a lowered thermal resistance for the device.

KEYWORDS: heat spreader, two-phase, high heat flux, carbon nanotube, sintered copper

NOMENCLATURE

A	cross-sectional area, m^2
d	mesh wire diameter, m
D_p	particle diameter, m
D_g	channel depth, m
h	heat transfer coefficient, W/m^{2}K
K	permeability, m^2
L	length, m
$\dot{m}$	mass flux, kg/s
ΔP	pressure differential, Pa
Q_{con}	condensation heat, W
r_{eff}	effective pore radius, m
t	thickness, m
ΔT	temperature differential, K
W	mesh opening, m
W_g	channel width, m

Greek symbols

ε	porosity
μ	viscosity, Pa s
ρ	mass density, kg/m^3
σ	surface tension coefficient, N/m
θ	contact angle

Subscripts

cap	capillary
con	condenser
eva	evaporator
l	liquid

INTRODUCTION

There is a growing need for effective thermal management of high-performance electronic devices. A common temperature-control solution is the use of a fan and heat sink to actively cool the heat source. Active liquid cooling systems are also receiving increased interest. These systems can generate even higher convection coefficients if combined with microchannels, or if two-phase flow is allowed to occur. In non-consumer devices such as lasers or concentrator photovoltaic systems, these liquid-circulating systems are regarded as the best solution. However, the pumping power required to support active liquid cooling systems is a major disadvantage.

The development of new cooling technologies that can manage high heat fluxes and reduce manufacturing cost while at the same time reduce power consumption by the thermal solution is highly desired. A vapor chamber is the most widely used example of a passive cooling device. Commercial vapor chambers can support heat fluxes of approximately 1 W/mm^2 [1]. Zhao *et al.* [2][3] developed a bi-dispersed wick structure which achieved a cooling rate of 3.3 W/mm^2. Many other wick structures have been reported in the literature, both in terms of detailed experimental results and analytical modeling efforts [4-22]. In addition, carbon nanotubes (CNTs) have been shown to enhance boiling heat transfer [23-27]. Few passively cooled devices offer heat dissipation levels approaching 5 W/mm^2. Cai *et al.* [28] developed a patterned CNT array evaporator surface that was shown to support a heat flux of 6 W/mm^2; however, such a surface was not incorporated into a device-level heat spreader.

978-1-4244-5343-6/10/$26.00 ©2010 IEEE

The purpose of the present work is to develop a two-phase heat spreader capable of removing greater than 5 W/mm^2 of heat flux from a device, and to experimentally demonstrate this performance.

HEAT SPREADER DESIGN

Reduction of the thermal resistance across the evaporator is a key bottleneck to achieving high heat flux passive cooling. A prototype heat spreader unit is developed with a provision for evaluating multiple evaporator surface designs. This prototype is depicted in Fig. 1.

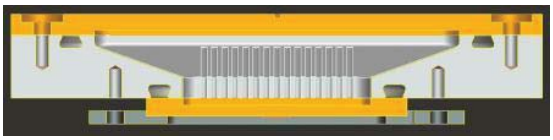

Fig. 1 Cross-sectional diagram of the prototype heat spreader.

The heat spreader is designed to be inserted into a thermal stack as a flat plate. The top surface serves as a condenser and the lower surface as an evaporator. The walls connecting the top and bottom are adiabatic and provide a fluid return path.

Condenser

The condenser plate is shown in Fig. 2. A screen mesh is attached to the condenser plate by diffusion bonding to assist in spreading the condensed liquid and to increase the condensation area. The active area of 70 mm x 70 mm is sufficient to support the condensation of 200 W of heat if the superheat temperature of the condenser is 2 K and the heat transfer coefficient is 2000 W/m^{2}K [29].

$$Q_{con} = hA\Delta T$$

$$A = \frac{Q_{con}}{h\Delta T} \cong 70\text{mm} \times 70\text{mm}$$

A thermocouple is attached at the center of the outer surface of the condenser plate.

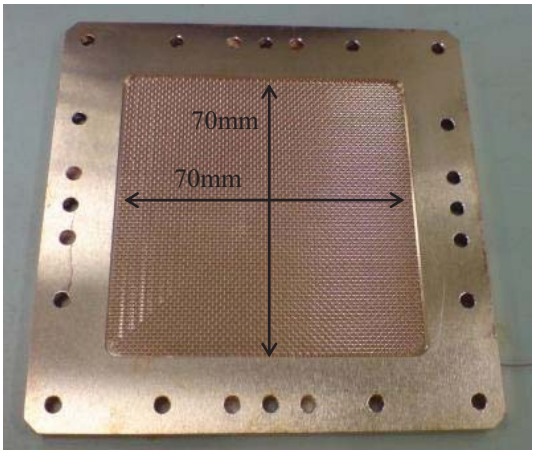

Fig. 2 Detailed view of the condenser plate at the top of the heat spreader.

The pressure drop in the screen mesh on the condenser surface [30] is estimated from

$$\Delta P_{con,l} = \frac{\mu_l \dot{m}_l L}{A\rho_l K} \qquad (1)$$

where $K = \frac{d^2\varphi^3}{122(1-\varphi)^2}$, $\varphi \approx 1 - \frac{1.05\pi Nd}{4}$, and $N = \frac{1}{W+d}$.

The pressure drop calculation assumes that four flow paths exist, as illustrated in Fig. 3. Each flow path has 10 mm width, 35 mm length and 0.48 mm depth.

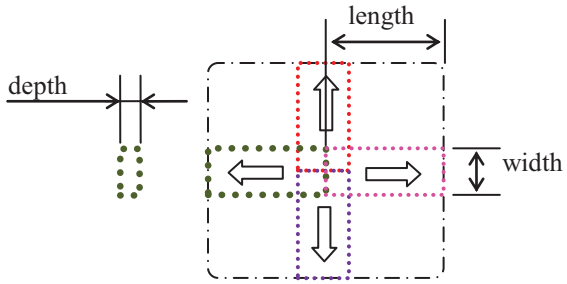

Fig. 3 Fluid flow paths assumed in prediction of the condenser section pressure drop.

For the design of the heat spreader in this study, the flow rate is estimated using the latent heat of water and an evaporation heat flow rate of 125 W (corresponding to a flux of 5 W/mm^2 over an area of 5 mm x 5 mm).

The capillary pressure drop in the condenser is given by

$$\Delta P_{con,cap} = \frac{2\sigma\cos\theta}{r_{eff}} \qquad (2)$$

$$r_{eff} = \frac{W+d}{2}$$

Based on this calculation, a screen with a mesh size of N = 30 was chosen.

Adiabatic fluid flow section

The middle part of the device is shown in the photograph in Fig. 4. A screen mesh is welded on the inside of the sloping side walls. Further, four rolled screen meshes are positioned on this wall mesh to ensure an adequate flow path between the condenser and the evaporator. In addition, 60 grooves are cut into the surface beneath the screen mesh by end milling. The pressure drop for flow through these grooves is estimated by treating the grooves as rectangular channels.

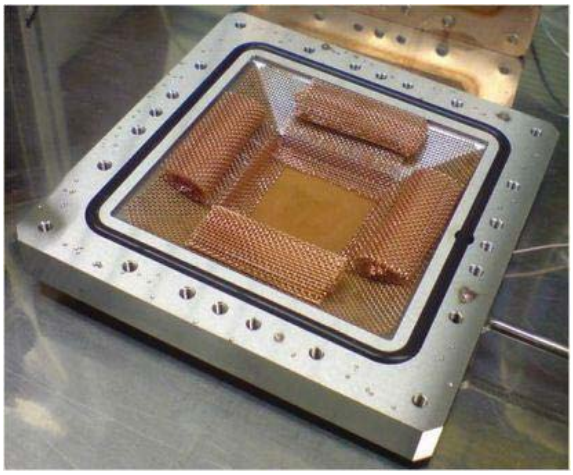

Fig. 4 Photograph of the adiabatic section.

Evaporator

The evaporator structure is the main focus of this study. While many enhanced evaporator structures have been explored in the literature, the structure of interest in the present work is an evaporator coated with an array of carbon nanotubes (CNT) operating under capillary-fed flow. Such a surface has been previously investigated in the literature, but for the enhancement of nucleate pool boiling. A sintered copper powder surface coated with a CNT array is developed in the present work for use as an evaporator. For the purposes of designing the heat spreader, however, the pressure drop through the wick and the capillary pressure provided by the wick are based on calculations for a screen mesh and bare sintered copper powder, and the effect of the presence of CNTs is not considered in these estimates. The flow in the evaporator is modeled in a manner similar to the illustration in Fig. 3. The flow length is 18 mm and the flow width is 7 mm. The depth is 0.05 mm for a #200 screen mesh and 1.5 mm or 0.5 mm for the sintered copper. The effective radius and the permeability of the sintered copper are calculated as shown below, with the diameter range of the copper particles being 38-63 μm.

$$r_{eff} = 0.21 D_p$$

$$K = \frac{D_p{}^2 \varepsilon^2}{150(1-\varepsilon)^2}$$

Estimation of the maximum heat flux

Using the equation (1) and (2), the required supply pressure can be calculated (in Pa) as

$$\Delta P = \Delta P_{eva,Cap} - \Delta P_{eva,l}$$

$$= \Delta P_l + \Delta P_{con,l} + \Delta P_{con,Cap} = 86 + 283 + 4 = 373$$

Therefore, the difference in the capillary pressure and the pressure drop in the system must be more than 373 Pa in order to circulate the working fluid in this device.

Table 1 gives the results of this estimation for the different evaporator wick structures investigated.

Table 1 Difference in pressure in case of each wick structure. The screen mesh and thick sintered wick show negative values which implies that they cannot support 5 W/mm^2 of input heat flux.

	$\Delta P_{eva,cap}$, Pa	$\Delta P_{eva,l}$, Pa	ΔP, Pa
#200 mesh	1895	3732	-1837
Thick sintered powder (1.5 mm)	11461	4072	7389
Thin sintered powder (0.5 mm)	11461	12216	-755

The thicker sintered powder evaporator is clearly the only candidate wick that can provide the appropriate fluid-feeding capable of providing 5 W/mm^2 of heat flux capability. It is estimated that the #200 screen mesh is capable of cooling 2.5 W/mm^2. Fig. 5 shows a picture of the actual device. The tubing on the side is used for evacuating the air, filling the working fluid, and draining excess liquid.

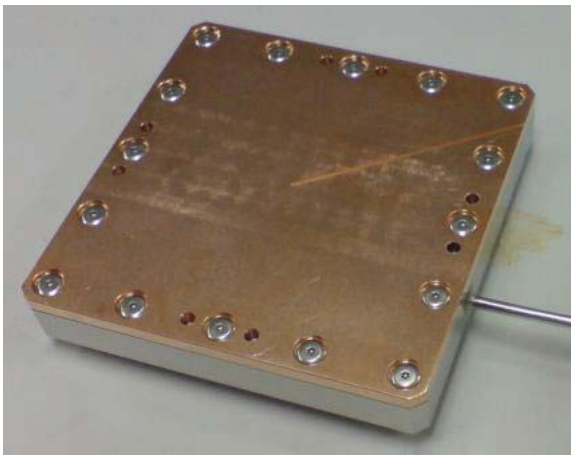

Fig. 5 Photograph of the assembled heat spreader.

EXPERIMENTAL SETUP AND SAMPLE FABRICATION

Heater Chip

This experiment requires a concentrated heat source that produces extremely high heat fluxes of greater than 5 W/mm^2. This was achieved using a patterned platinum film as shown in Fig. 6. The resistance of the heater so fabricated is 120 Ω.

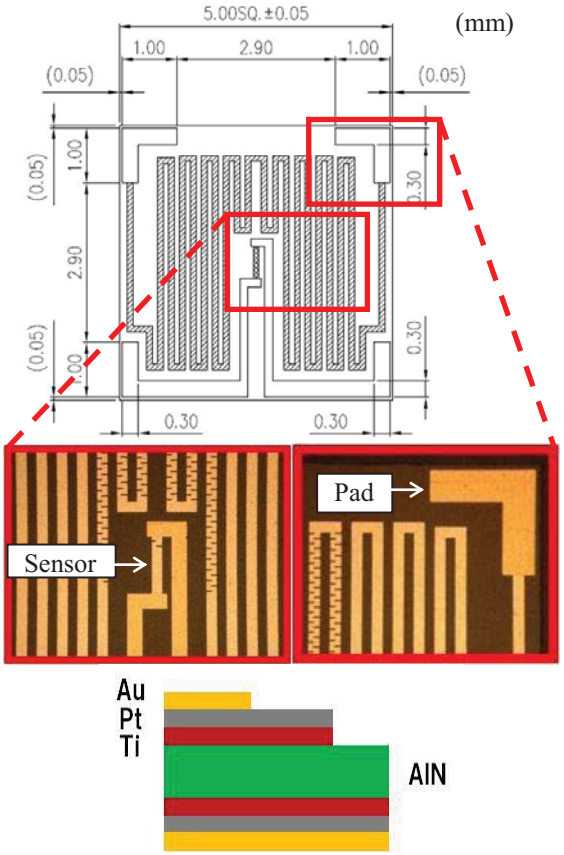

Fig. 6 Detail of the heat source: plan view and cross-section of the layered structure.

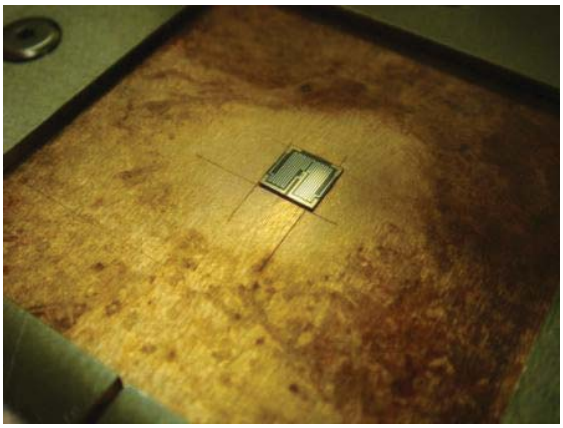

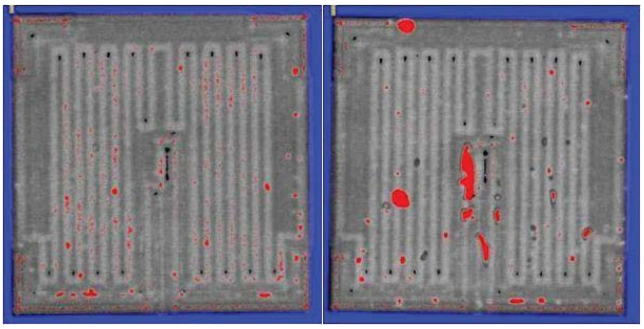

Fig. 7 Photograph of the heat source after soldering to the evaporator substrate and quality of solder joint as revealed by scanning acoustic tomography.

The central pattern in the heat source acts as a temperature sensor. The temperature of the heat source is detected by the change in its electrical resistance. This chip is soldered to the evaporator substrate as shown in Fig. 7 using Au80Sn20 (melting temperature: 278 °C).

A quantitative evaluation of possible void areas in the solder joint was performed using scanning acoustic tomography (SAT). The observed examples are shown in Fig. 7, with the red areas indicating voids. The evaluation ensures that the void areas comprise less than 5% of the total area. The lead wires powering the heat source are shown in Fig. 8.

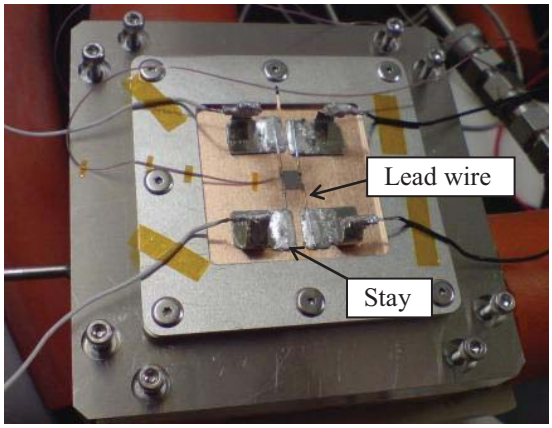

Fig. 8 Image of the back side of the heat spreader showing the heat source.

The heat loss from the back side of the heat source must be quantified in order to predict the heat flux provided to the evaporator. Heat loss was estimated as illustrated in Fig. 9.

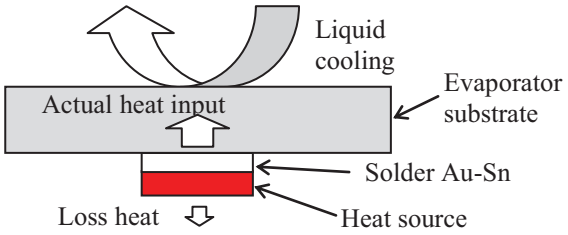

Fig. 9 Schematic approach for heat loss evaluation.

The actual heat supplied to the evaporator substrate can be found by measuring the temperature rise of the liquid between inlet and outlet of the cold plate. Results of the heat loss estimation are shown in Fig. 10, which shows a heat loss of approximately 14% of the supplied electrical power.

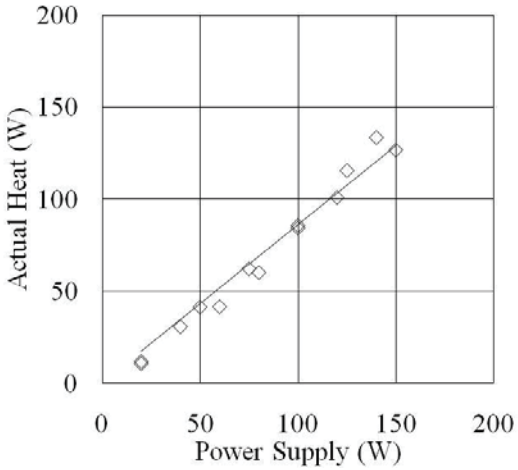

Fig. 10 Relationship between supplied heat and that which enters the heat spreader.

The temperature of the sensor is calibrated in a furnace. As shown in Fig. 11, the resistance of the temperature sensor in the heat source was found to vary linearly with temperature. The temperature is measured by the thermocouple on the heat source.

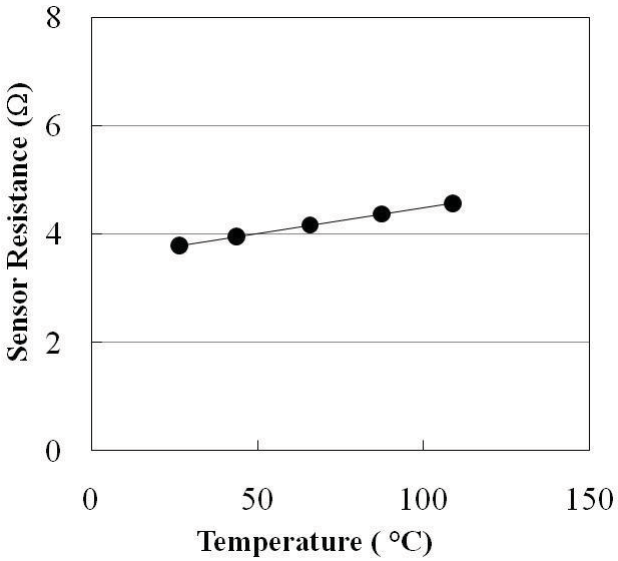

Fig. 11 Calibration data for the temperature sensor. The temperature value on the x-axis indicates the measurement from a thermocouple attached to the heater chip.

Experimental setup

The exposed surface of the condenser plate of the heat spreader is attached to a water-cooling jacket to reject the heat from the device. The interface conductance is improved using grease and 40 °C cooling water is circulated through the jacket. Therefore the condenser temperature is approximately 40 °C. Fig. 12 shows an image of the assembled test setup including the jacket and insulation. After mounting, the heat spreader is first evacuated and is then charged with the working fluid, pure water, up to full capacity. The amount of water and the inside pressure are then reduced in small steps by heating. The ideal amount of charge is different for each heat flux, and therefore, different amounts of charge were used in different test samples. Any extra liquid degrades the heat transfer coefficient in evaporation and condensation.

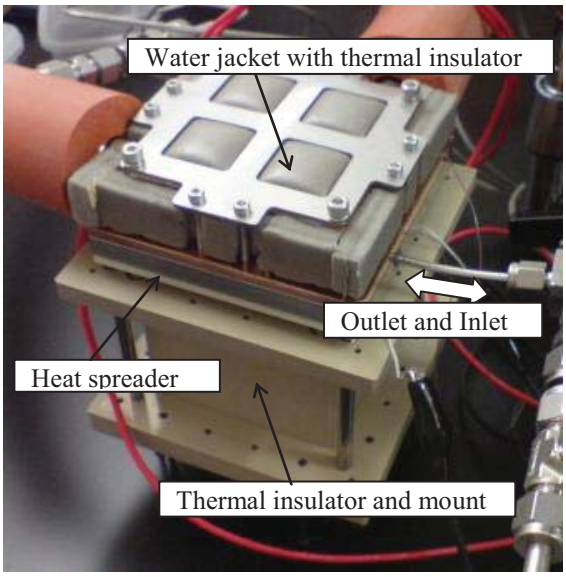

Fig. 12 Photograph of the assembled experimental setup.

Evaporator surface preparation

The screen mesh evaporator was attached to the evaporator substrate by diffusion bonding. This mesh was made of oxygen-free copper. For the sintered sample, sintering was performed in a furnace at 950°C in an argon atmosphere [31]. Both samples are shown in Fig. 13.

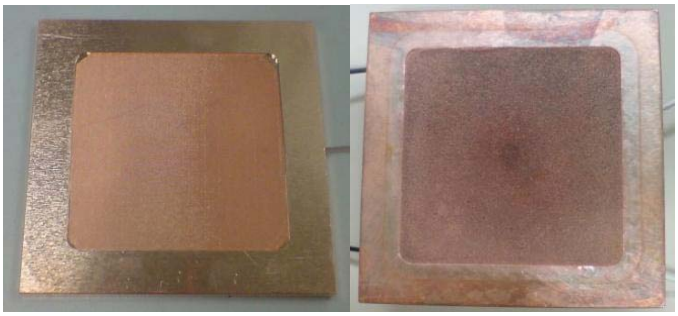
Fig. 13 Screen mesh evaporator (left) with mesh number of #200 and thickness 0.1 mm. Sintered copper evaporator (right) of particle size 50 μm diameter and thickness 1.5 mm.

CNTs were deposited on to the sintered copper substrate from ethanol by thermal chemical vapor deposition. A catalyst layer prepared by sputtering Fe/Al /Al_2O_3 ensured good CNT growth and anchoring. The CNT evaporator is shown in Fig. 14. The multi-walled CNTs fabricated by this process were estimated from SEM images to be 20-25 μm long and 50-100 nm in diameter. The CNTs, which are hydrophobic as fabricated, were exposed to ultraviolet radiation which damage the surface of the CNTs and render them hydrophilic. This is a critical requirement for the current application.

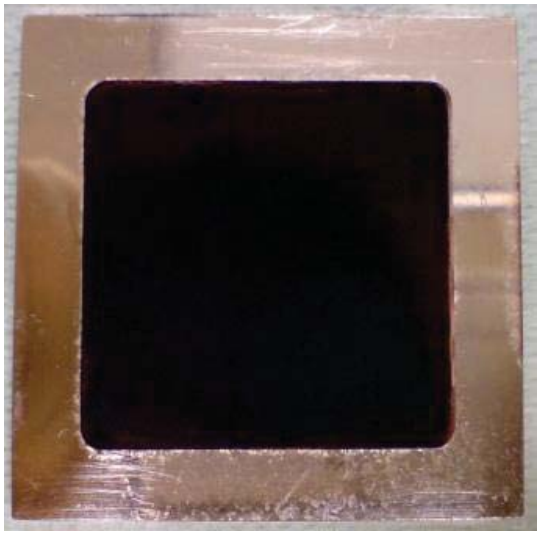

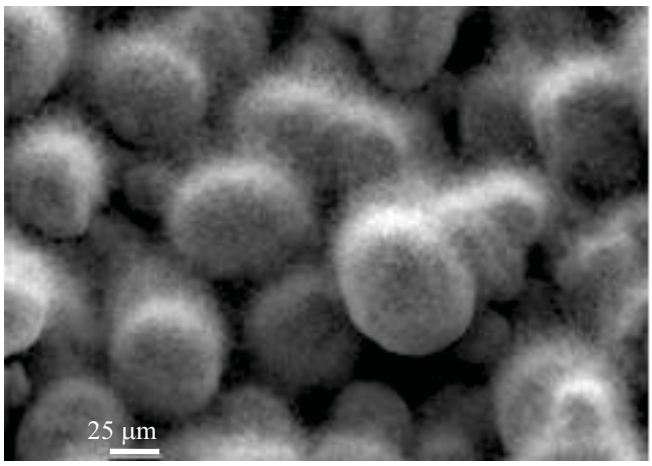

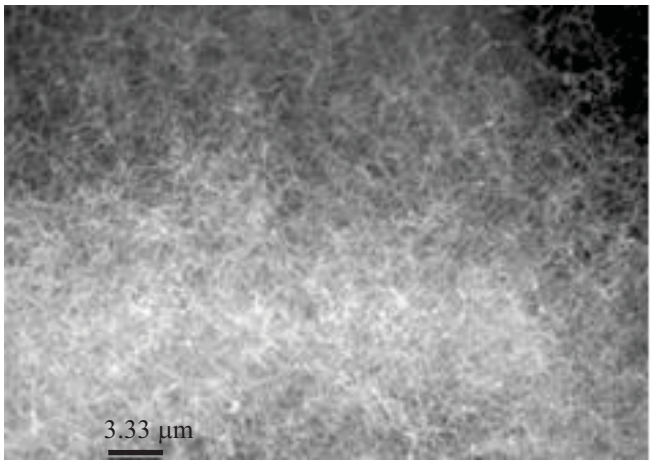

Fig. 14 CNT-coated sintered copper evaporator (top); SEM image of CNT-coated sample (middle); and magnified SEM image of CNT-coated sample (bottom).

TEST RESULTS

The measured thermal characteristics of the three types of evaporator are described in this section. The superheat temperature in these results is defined as the difference between the heat source sensor temperature and the condenser temperature. The condenser temperature is measured by a thermocouple mounted on the outside of the condenser plate. Fig. 15 shows that the screen mesh evaporator can support a little more than 2 W/mm^2. Heat fluxes above 2.1 W/mm^2 could not be tested because the resulting temperature exceeded the melting point of the solder; this heat flux, therefore, is not the dry-out limit for this surface. The superheat temperature was 185°C at 2 W/mm^2. This superheat is excessive for cooling an electronic device.

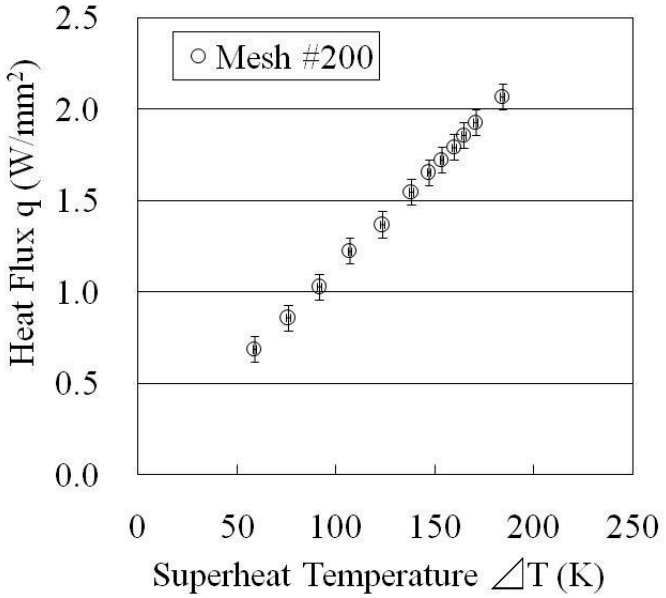

Fig. 15 Thermal performance of the screen mesh evaporator. The maximum value of 2.1 W/mm^2 is not indicative of dry-out, but instead discontinuation of the test due to the melting point of the solder having been reached.

Fig. 16 shows test results for a sintered copper powder evaporator and showcases the excellent performance of this surface for a heat spreader application. The device was able to dissipate 8.5 W/mm^2. Even beyond this flux, it is not dry-out which limits the performance of this surface, but instead damage to the heat source wires, which burned out at 9 W/mm^2. In addition, this sample used a larger charge of water in order to accommodate a higher heat flux, which leads to a higher superheat.

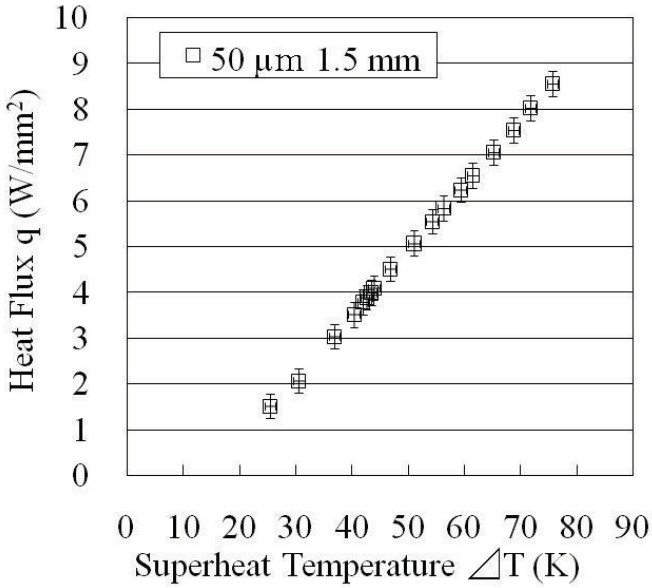

Fig. 16 Thermal performance of the sintered copper evaporator. The maximum value of 8.5 W/mm^2 is not indicative of dry-out, but instead discontinuation of the test due to damage to the heat source wire.

It is interesting to note that the analysis in Table 1 indicates that the thin sintered evaporator could not handle 5 W/mm^2. However, the experiments show that the sample was able to readily dissipate this amount of heat. The apparent discrepancy is likely due to the simplified modeling of the flow path in the condenser and evaporator.

As a result of the good performance of the thin sintered sample, this sample was selected to be coated with CNTs. Fig. 17 shows the effects of the added CNT array. In this case, the amount of working fluid used to charge the heat pipe was adjusted for a heat input of 5 W/mm^2. Comparing the sintered copper with and without CNTs, the CNT-coated sample supports higher heat fluxes at a given superheat than the bare sample. At a given heat flux, the CNT-coated sample operates at a superheat that is more than 10 K lower than that of the uncoated sample. The thermal resistance of the coated sample is 0.27 K/W, while the uncoated sample shows a resistance of 0.37 K/W. These thermal resistances are based on an input heat flux of 5 W/ mm^2.

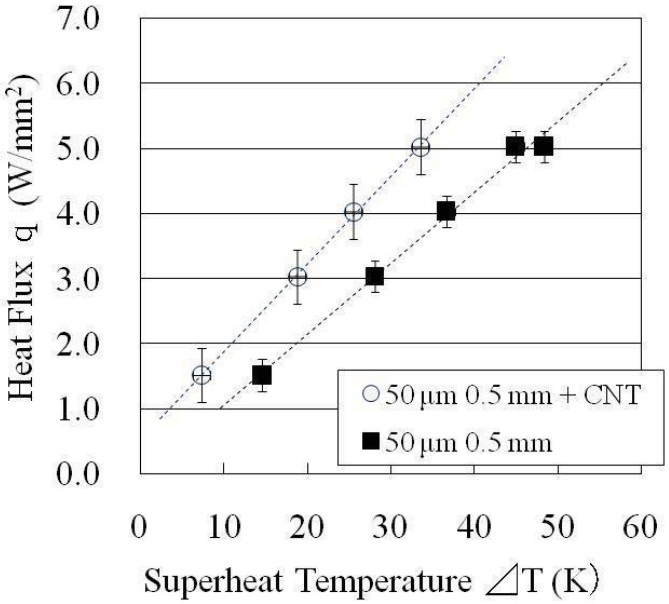

Fig. 17 Comparison between the CNT-coated and bare sintered powder evaporator.

CONCLUSIONS

A two-phase heat spreader for ultra-high heat flux applications was developed, as was an experimental facility for evaluating its performance. The results from the experimental investigation revealed that the heat spreader device can dissipate up to 8.5 W/ mm^2 using a sintered powder wick evaporator structure. Coating the sintered powder evaporator with a hydrophilic CNT array reduced the temperature drop across the evaporator by as much as 10K for a given heat flux.

ACKNOWLEDGEMENTS

The authors express their gratitude to Prof. Tim Fisher, Prof. Jayathi Murthy, Ram Ranjan, and Glen Powell of Purdue University for their support of this study.

REFERENCES

[1] http://www.fujikura.co.jp/00/news/0310/news2.html

[2] Zhao, Y. and Chen, C., 2007, "Vaporization Heat Transfer in Sintered Copper Wicks with Micro-grooves in Heat Pipe Evaporators," Thermal Challenges in Next Generation Electric Systems THERMES 2007, Miillpress, pp. 241-247

[3] Zhao, Y. and Chen, C., 2006, "An Investigation of Evaporation Heat Transfer in Sintered Copper Wicks With Microgrooves," Proceedings of IMECE2006, Chicago

[4] Li, C. and Peterson, G. P., 2006, "Comprehensive Comparisons between Evaporation and Pool Boiling on Thin Micro Porous Coated Surfaces," Proceedings of IMECE2006, Chicago

[5] Li, C., Peterson, G. P. and Wang, Y., 2006, "Evaporation/Boiling in Thin Capillary Wicks- Wick Thickness Effects," ASME Journal of Heat Transfer, 128, pp.1312-1319

[6] Li, C. and Peterson, G. P., 2006, "Evaporation/Boiling in Thin Capillary Wicks-Effects of Volumetric Porosity and

Mesh Size," ASME Journal of Heat Transfer, 128, pp.1320-1328
[7] Hasebe, S., Shikazono, N. and Kasagi, N., 2004, "Modeling and Design of Micro Groove Falling Film Evaporators," ICMM2004, New York
[8] Hasebe, S., Shikazono, N. and Kasagi, N., 2004, "Modeling and Design of Micro Groove Falling Film Evaporators," National Heat Transfer Symposium of Japan, pp.405-406
[9] Suehisa, Y., Shikazono, N., Kasagi, N. and Iwata, H., 2005, "Study on Micro-Grooved Plate Evaporator," 42nd National Heat Transfer Symposium of Japan, pp.543-544
[10] Wang, H., Garimella, S. V. and Murthy, J. Y., 2007, "Characteristics of an evaporating thin film in a microchannel," International Journal of Heat and Mass Transfer, 50, pp.3933-3942
[11] Wang, J. and Catton, I., 2001, "Enhanced evaporation heat transfer in triangular grooves covered with a thin fine porous layer," Applied Thermal Engineering, 21, pp.1721-1737
[11] O'Connor, J. P., You, S. M. and Price D., 1995, "A Dielctric Surface Coating Technique to Enhance Boiling Heat Transfer from High Power Microelectronics," IEEE Transaction on Components, Packaging, and Manufacturing Technology-Part A, 18-3, pp.656-663
[14] Mughal, M. P. and Plumb, O. A., 1996, "An experimental study of boiling on a wicked surface," International Journal of Heat and Mass Transfer, 39, pp.771-777
[15] Semenic, T., Lin, Y. and Catton, I., 2005, "Biporous Sintered Copper for a Closed Loop Heat Pipe Evaporator," Proceedings of IMECE2005, Orlando
[16] Abhat, A. and Seban, R. A., 1974, "Boiling and Evaporation from Heat Pipe Wicks With Water and Acetone," Journal of Heat Transfer, 96, pp.331-337
[17] Chang, J. Y. and You, S. M., 1997, "Boiling heat transfer phenomena from microporous and porous surfaces in saturated FC-72," International Journal of Heat and Mass Transfer, 40, pp.4437-4447
[18] Nakayama, W., Daikoku, T., Kuwahara, H. and Nakajima, T., 1980, "Dynamic Model of Enhanced Boiling Heat Transfer in porous Surfaces Part 1: Experimental Investigation," Journal of Heat Transfer, 102, pp.445-450
[19] Iverson, B. D., Davis, T. W., Garimella, S. V. and North, M. T., 2007, "Heat and Mass Transport in Heat Pipe Wick Structures," Journal of Thermophysics and Heat Transfer, 21, pp.392-404
[20] Vityaz, P. A., Konev, S. V., Medvedev, V. B. and Sheleg, V. K., 1984, "Heat Pipes with Bidispersed Capillary Structures," The proceedings part 1of 5th International Heat Pipe Conference, Tsukuba
[21] North, M. T., Sarraf, D. B., Maidanik, Y. F. and Vershinin, S., 1997, "High Heat Flux Loop Heat Pipes," 6th European Symposium on Space Environmental Control Systems, Netherlands
[22] Liter, S. G. and Kaviany, M., 2001, "Pool-boiling CHF enhancement by modulated porous-layer coating: theory and experiment," International Journal of Heat and Mass Transfer, 44, pp.4287-4311
[23] Zhou, J. J., Noca, F. and Gharib, M., 2007, "Flow Conveying and Diagnosis with Carbon Nanotube Arrays," Nanotechnology, 17, pp.4845-4853
[24] Launay, S., Fedorov, A. G., Joshi, Y., Cao, A. and Ajayan, P. M., 2006, "Hybrid Micro-nano Structured Thermal Interfaces for Pool Boiling Heat Transfer Enhancement," Microelectronics Journal, 37, pp.1158-1164
[25] Ahn, H. S., Sinha, N., Zhang, M. and Baughman, R. H. 2006, "Pool Boiling Experiments on Multiwalled Carbon Nanotube (MWCNT) Forests," Journal of Heat Transfer, 128, pp.1335-1342
[26] Ujereh, S., Fisher, T. S. and Mudawar, I., 2007, "Effects of Carbon Nanotube Arrays on Nucleate Pool Boiling," International Journal of Heat and Mass Transfer, 50, pp. 4023-4038
[27] Ujereh, S., Mudawar, I., Amama, P. B. and Fisher, T. S., 2005, "Enhanced Pool Boiling Using Carbon Nanotube Arrays on a Silicon Surface," Proceedings of IMECE 2005, pp.691-696
[28] Cai, Q., Zhao, Y., Tsai, C., and Chen C., 2009, "Investigation of High Heat Flux Cooling Using Carbon Nanotube Bi-wick Structure and Integrated Platinum Thermometer /Hearer," Proceedings of the ASME 2009 Heat Transfer Summer Conference
[29] Aihara, T., 1994, "DENNETSU KOUGAKU," SHOKABO, pp.172 (in Japanese)
[30] Faghri, A., 1995, "Heat Pipe Science and Technology," Taylor&Francis
[31] Dunn, P. D. and Reay, D. A., 1994, "Heat Pipes Fourth Edition," Pergamon, pp. 172-173